

Design Aspects of Conductive Microfiber Rings for Shaft Grounding Purposes

Annette Muetze
University of Warwick
Coventry, CV4 7AL, GB-England
a.muetze@warwick.ac.uk

H. William Oh
Electro Static Technology
Mechanic Falls, ME, 04256, USA
hwoh@est-static.com

Abstract—Carbon brushes using electrically conductive carbon graphite have been used for shaft-grounding and current-conduction purposes for a long time. We present an alternative brush concept made from millions of conductive microfibers. If properly designed, such brushes can meet all the demands on carbon brushes but exclude the problems of excessive wear and hot-spotting/thermal wear commonly quoted with the first. These brushes have negligible frictional wear, are free of maintenance, and robust towards contamination. In addition, they are especially suitable for use with high-frequency currents and voltages, as they also allow current-conduction based on electric field emission. We develop the design criteria for such brushes both for prevention of voltage build-up and current-conduction of several 10s of Amperes with frequencies in the MHz range. We support the theoretical results with measurement results taken at different rotor shaft speed.

Index Terms—bearings (mechanical), common-mode voltage, electric breakdown, electric field effects, variable-speed drives.

I. INTRODUCTION

Carbon brushes using electrically conductive carbon graphite have been used for shaft-grounding and current-conduction purposes for a long time. With such brushes, a graphite film deposits on the contact area during sliding. Humidity creates a water layer on the graphite, thereby rendering the brushes self-lubricating. Commonly quoted problems are excessive wear and hot-spotting/thermal moulding as the contact is transferred to fewer, expanded, more fragile spots during the sliding, as well as brush dusting/low humidity lubrication [1]. When being used with applications where high-frequency voltages and currents occur, maintaining good electrical contact poses additional challenges on the design and installation of such conventional brushes. Such applications are for example given when the brushes are being used as mitigation technique for inverter-induced high-frequency bearing currents.

In this paper, we present an alternative brush concept made from millions of conductive microfibers. If properly designed, such brushes can meet all the demands on conventional carbon brushes but they have negligible frictional wear, are free of maintenance, and robust towards contamination. In addition, these microfibers also allow current-conduction based on electric field emission. They are therefore especially suitable for use with high-frequency currents and voltages. Thereby, they present a cost-effective option for a mitigation technique for inverter-induced bearing currents. While presenting this brush concept, we focus on the design criteria for such brushes for use with different drive configurations. Thereby, the two different primary purposes, (A) current-conduction and (B) prevention of voltage build-up, are both considered. It is shown (A) how currents of several 10s

of Amperes can be carried and (B) how voltages as low as a few Volts can be discharged, both with frequencies in the MHz range. The theoretical results are confirmed with measurement results taken with different drive configurations and set-ups. The application of such brushes as mitigation technique for discharge bearing currents itself, which is closely related to (B), was discussed in a previous publication [2]. This paper focuses on the application of conductive microfiber rings in a broader sense. Where appropriate for comprehensiveness, findings presented in [2] are briefly reviewed.

The paper is organized as follows: First, the concept of the conductive microfiber rings is explained (Section II). Then, a concise summary of the required background information of electric discharge (ESD) effects (Section III) and a brief review of inverter-induced bearing currents (Section IV) are given, and the orders of magnitudes of the currents and voltages that determine the requirements on the brushes are derived (Section V). In the main part of the paper, the theory of the proposed technique is discussed (Sections VI and VII) and measurement results are presented (Section VIII). Conclusions are drawn at the end of the paper (Section IX).

II. CONDUCTIVE MICROFIBER RINGS: THE CONCEPT

The proposed new brush concept can fulfil the same functions as conventional carbon brushes. That is, they can (A) carry current of significant magnitude and/or (B) prevent voltage build-up. However, in contrast to the spring-loaded mechanism of conventional carbon brushes, the technique has no direct frictional wear, is maintenance-free, robust towards contamination, and thus it is free of the problems that are commonly quoted with brushes (Section I).

In general terms, brushes are used to establish an electric contact between two conductive elements, where one is at rest and one is moving, in most cases rotating. In the context of electric drives, these are in most cases the stator and the rotating motor shaft, respectively. The challenge of maintaining good electric contact is directly related to the movement involved: On the microscopic level, the distance between the stationary and rotating elements, here the stator and the rotor, is not constant but varies with surface roughness and centering/alignment. With conventional carbon brushes, this challenge is addressed via the initial tension of the spring.

Here, we propose an alternative approach to establish electric contact between two elements as described above that uses *conductive microfibers*. These are fibers with strands less than one

denier, where one denier equals 1 gram per 9 000m of fiber. They have very small diameters of less than $10\mu\text{m}$ and are mechanically flexible and yet high strength, high stiffness fibers. If applied with the correct interference, these microfibers can maintain contact with the surface, thereby compensating surface roughness and/or microscopic variations of the distance resulting from non-ideal centering/alignment. In spite of the rotating movement of the shaft, the microfibers only “see” one non-rotating second pole, and the rotation of the machine shaft does not affect the functional capability of the fibers. When the microfibers lose “good” electric contact by mechanical contact, a breakdown due to local field emission will occur somewhere along the circumference, thereby reestablishing the electric contact. If properly designed, these fibers

- (A) carry current (either directly for current-carrying purposes or to prevent voltage build-up across a parallel impedance).
- (B) lead to a breakdown the moment a “good” electric contact between the fibers and the shaft is lost.

When a multitude of such fibers is assembled around a machine shaft, a high density of contact points is given, and many parallel paths either for (A) or for (B) are provided.

If properly designed, the interference between the fibers and the shaft can have ultra-low friction, giving a technique that is free of direct frictional wear. Furthermore, the fibers can be designed to cut through contaminants such as given by oily, greasy, moist, and dusty environments. The fibers can be assembled to give a ring with a rather slim design that can be mounted on both the nondrive- and drive-end of a machine with rigid mounting plates or mounting brackets, where the electric contact is ensured with screws. Thereby, no machining is required, and the installation of the device is relatively simple. The close views of two realizations of such rings of conductive microfibers and a ring as it is mounted on a machine are shown in Figs. 1 and 2 respectively.

III. BACKGROUND FOR (B): THE MODIFIED PASCHEN CURVE

A. Gaseous discharge for “large” gaps (above $\approx 5\mu\text{m}$)

Gaseous breakdown at “large” gaps is commonly described using the Paschen curve that is based on Paschen’s law [3]. The Paschen curve correlates the breakdown voltage V_B and the reduced variable $\rho = p \cdot d$, where p is the pressure and d is the gap spacing. For each pressure-gap product, it predicts a minimum breakdown voltage, the so-called Paschen-minimum (Fig. 3). The underlying understanding of the breakdown mechanism is the Townsend (avalanche) breakdown in gases. That is, the cascading effect of secondary electrons obtained by collisions and impact ionization of the gas ions accelerating across the gap [4], [5]. The breakdown voltage is affected by the geometrical configuration of a discharge gap, particularly, the shape and the size of the electrodes used in the tests [6], [7]. Breakdown for gaps greater than approximately $10\mu\text{m}$ has been well studied and the breakdown limit for air at one atmosphere identified to $3\text{V}/\mu\text{m}$ ($3\text{kV}/\text{mm}$). The minimum breakdown voltage is approximately 360V and occurs at a gap spacing of $5\mu\text{m}$ and it *increases* for smaller gaps [8]. In contrast to a widespread misconception,



Fig. 1. Multitudes of conductive microfibers assembled in rings to give conductive microfiber rings.

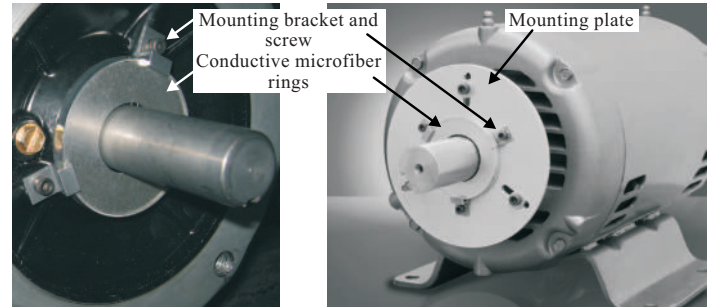


Fig. 2. Conductive microfiber rings mounted at machine shafts (four-pole squirrel-cage induction motors with IHP rated power and 143TC frame).

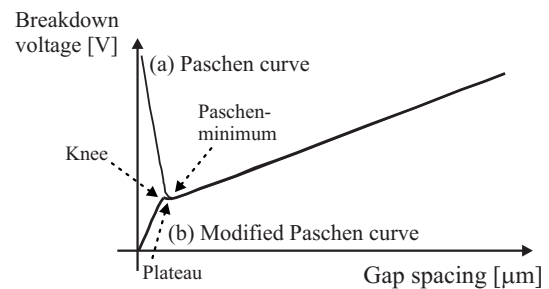


Fig. 3. Qualitative sketch of (a) the Paschen curve and (b) the modified Paschen curve based on [9].

the same breakdown mechanism does not hold for smaller gap spacings [8]: The left, rising part of the Paschen curve is not observed for air gaps at atmospheric pressure [9]. A statement that is also supported by the 80V breakdown voltage reported for a $0.12\mu\text{m}$ air gap in [10].

B. Electric field emission for “small” gaps ($\approx 5\text{nm}$ to $\approx 5\mu\text{m}$)

Field emission is a form of quantum tunneling and is also known as Fowler-Nordheim (F-N) tunneling [11]–[13]. It is the process whereby electrons tunnel through a barrier in the presence of a high electric field (that is often associated with a deformed surface potential barrier). The potential at which the electrons have sufficient kinetic energy to do so is commonly referred to as barrier gap or work function potential. As the kinetic energy of the charge carriers has a certain distribution over the population, some of them have enough energy to cross the gap even much below the breakdown voltage. In contrast to the Frenkel-Powl

tunneling commonly used for semiconductor devices, the F-N tunneling does not rely on defects in a material.

An important parameter in this context is the field enhancement factor, commonly denoted β . It includes the enhancement of the electric field due to the geometry, β_g , and due to the microscopic peaks in the (polished!) contact surface, β_m , and can reach more than two orders of magnitudes [15]. Then,

$$V = d \cdot \frac{E_m}{\beta}, \quad (1)$$

where E_m is the microscopic electric field strength at the microsurface of the contact, and V and d are the voltage and the distance respectively.

The electrons resulting from field emission can initiate an electric breakdown that occurs when the (local) field emission current density (at microscopic level) exceeds a critical value [15]. This breakdown due to the field emission effect occurring at smaller gaps is included in the little-known *modified* Paschen curve [9]. It is best explained by quoting the authors of [8]:

“The modified Paschen curve shows a platform where the pure Paschen curve would have a minimum which is interpreted as the transition region between the gaseous Townsend avalanche and field emission induced breakdown. For smaller gaps (left) of the plateau, breakdown is only due to field emission. The breakdown voltage drops to zero. Details of the geometry and the metal electrode properties influence the exact location of the transition.”

C. Summary of key qualitative results

1) Metal-air-metal [8]:

$V_B/d = 156\text{V}/\mu\text{m}$ (conservative estimate, neglecting the influence of the curvature and the film); breakdown voltages 151V and 135V (two samples), $0.9\mu\text{m}$ gap; glass deposited on a 100nm thick chrome and a chrome finger with $2\mu\text{m}$ diameter. The modified Paschen curve was obtained for gap spacings between $0.9\mu\text{m}$ and $4.0\mu\text{m}$, where the knee was found at $2\mu\text{m}$. The field emission behavior was confirmed via the F-N plot.

2) Metal-air-metal [15]:

$V_B/d = 110\text{V}/\mu\text{m}$ and $V_B/d = 65\text{V}/\mu\text{m}$ from data obtained by the authors of [16] and [17]; [16]: Fe polished needle with 0.6mm diameter, 0.05mm radius, and silver disc, gap spacings $0.2\mu\text{m}$ to $40\mu\text{m}$; [17]: very carefully developed contact system, clean room measurements, Ni, Al, and brass contacts—no difference in V_B was found, showed that Paschen’s law is not applicable for gaps between 0 and $4\mu\text{m}$.

IV. REVIEW: CLASSIFICATION OF INVERTER-INDUCED BEARING CURRENTS

If no additional measures like special filters or control schemes are applied, a voltage-source inverter presents a high-frequency voltage source in the common-mode circuit. The generated common-mode voltage contains high-frequency components that interact with capacitances inside the machine that have not been

of influence at line-operation. As a result, different inverter-induced bearing currents can occur that can be classified as follows:

- 1) Small capacitive bearing currents (usually considered not dangerous to the bearings, therefore, not discussed further.).
- 2) Discharge bearing currents (also: “EDM (Electric Discharge Machining) bearing currents”).
- 3) High-frequency circulating bearing currents.
- 4) Bearing currents due to rotor ground currents.

The first two are related to the influence of the high-frequency common-mode voltage, v_{com} , on the voltage across the bearing, v_{bea} . The last two are caused by high-frequency common-mode currents, i_{com} , that result from the interaction of v_{com} with high dv/dt and the capacitance between stator winding and motor frame, C_{wf} , (Fig. 4). For further information on the cause-and-effect chains, physical explanations, and possible mitigation techniques we refer to the literature, e.g. [18]–[26].

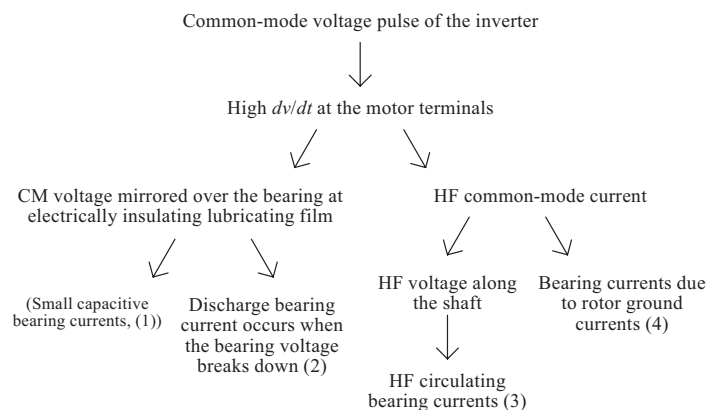


Fig. 4. Classification of the different types of inverter-induced bearing currents of inverter-based drive systems as a function of the different cause-and-effect chains.

As explained at the beginning of the paper, we consider two different primary purposes of the microfiber rings, (A) current-conduction and (B) prevention of voltage build-up. We select the field of inverter-induced bearing currents as application to show (A) how currents of several 10s of Amperes can be carried and (B) how voltages as low as a few Volts can be discharged, both with frequencies in the MHz range. To this aim, we next develop the orders of magnitudes of the relevant parameters as they can occur in this context (Section V).

V. ORDERS OF MAGNITUDES

A. Currents

The high-frequency common-mode voltage at the motor terminals causes—mainly because of the stator winding-to-frame capacitance, C_{wf} —an additional high-frequency common-mode current, i_{com} . For the purpose of straightforwardness, we use a very simplified model to estimate the amplitude of the high-frequency common-mode current, and we analyze each switching instant individually. We do not consider superposition of currents resulting from two consecutive switching instants at different

phases as the time-lag between two switching instants is generally larger than the characteristic time constant of the high-frequency common-mode current. Assuming the worst-case of an undamped system, the maximum amplitude of the high-frequency common-mode current, I_{com} , is then given by (2)

$$I_{com} = 2 \cdot dv_{Lg}/dt \cdot C_{wf}, \quad (2)$$

where dv_{Lg}/dt is the dv/dt of the voltage between the motor terminal connection (“line”) and the ground. Table I gives an overview of the ranges of I_{com} for different values of dv_{Lg}/dt and C_{wf} as they are typical for drive systems up to several hundreds of kW.

TABLE I

RANGES OF THE HIGH-FREQUENCY COMMON-MODE CURRENTS

dv_{Lg}/dt kV/ μ s	$C_{wf}^{(*)}$ nF	$I_{com}^{(**)}$ A	$0.1I_{com}$ A	$0.35I_{com}$ A
0.5	2...30	2...30	0.2...3.0	0.7...10.5
1.0	2...30	4...60	0.4...6.0	1.4...21
2.0	2...30	8...120	0.8...12	2.8...42

$^{(*)}$ Phase value, $^{(**)}$ $I_{com} = 2 \cdot C_{wf} \cdot dv_{Lg}/dt$.

Depending on the grounding connections of the drive, this current can return—partially or, in the most extreme case completely—to ground through the rotor, thereby passing through the bearing, if no additional measures are taken.

The high-frequency common-mode current also excites a circular magnetic flux around the motor shaft that induces a shaft voltage v_{sh} along the shaft.¹ If large enough to destroy its insulating properties, it can cause a high-frequency circulating bearing current. The ratio between the bearing and common-mode current depends on different parameters such as machine size and geometry and frequency content of the currents and is typically in the order of 10 to 20% with an upper bound of 35% [28] for “typical machines.” For illustration, the values of $0.1I_{com}$ and $0.35I_{com}$ are also included in Table I.

B. Voltages

At electrically insulating (“intact”) lubrication film, the voltage across the bearing, v_{bea} , mirrors the common-mode voltage, v_{com} (Fig. 5) via the capacitive voltage divider “Bearing Voltage Ratio” (BVR) (e.g. [19], [20]). The BVR is typically in the order of several %, with an upper bound of 10% for “typical” machines [27]. Table II gives an overview of the ranges of the maximum voltage across the bearing for different 3ph supply voltages and $BVR = 1\% \dots 10\%$. Increased voltage at the motor terminals due to voltage reflection can increase these values additionally.

VI. THE PROPOSED CONCEPT IN THEORY - PART I

A. Current-carrying capabilities

To assess the orders of magnitudes that affect the fiber design, we first consider the current-carrying capability of the fibers. To this aim, we approximate the current density of the fibers with

¹Note that the voltage across the bearing, v_{bea} , which has a very different nature, is also frequently referred to as “shaft voltage” in the literature.

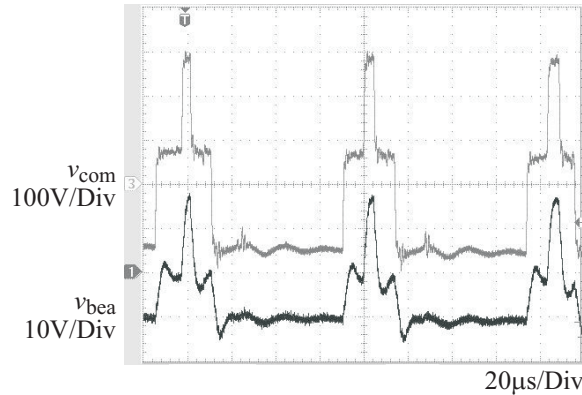


Fig. 5. At electrically insulating lubrication film, the voltage across the bearing (v_{bea}) mirrors the common-mode voltage (v_{com}); squirrel-cage induction motor, 215TC frame, 10HP rated power, motor speed 1800r/min.

TABLE II

RANGES OF THE VOLTAGE ACROSS THE BEARING

Supply voltage (3ph) (line-to-line, rms) V	Inverter dc-link voltage $^{(*)}$ V	Peak CM voltage $^{(**)}$ V	Voltage across bearing (BVR = 0.01...0.1) $^{(***)}$ V
200	270	180	1.8...18
240	324	216	2.2...22
380	513	342	3.4...34
460	621	414	4.1...41

$^{(*)}V_{dc} = \frac{3}{\pi} \sqrt{2} V_{LL,rms,1}$, $^{(**)}v_{com,pk} = \frac{2}{3} V_{dc}$, $^{(***)}v_{bea,pk} = BVR \cdot v_{com,pk}$

10^{10}A/m^2 , using [15] as starting point. This is a conservative estimate, and it is the current density before collapse (electric breakdown). Furthermore, with the surface area $S = \pi dl$ and the cross-sectional area $A_c = \pi d^2/4$, a multitude of N microfibers with total cross-sectional area NA_c has \sqrt{N} the surface area than a single fiber with the same surface area. Therefore, the heat dissipation is improved, allowing for higher current densities than would be possible with a single-conductor device. The heat generation in the microfiber rings eventually depend on the resistivity of the microfibers, which will be discussed below (Section VI-C). It is noteworthy that, at the high current densities of the microfibers, the heat generation and current-carrying capability of the structure for microfiber assembly will also be of importance.

As it is our intend to identify the orders of magnitudes and bounds, we continue the line of argument with the above mentioned estimate of 10^{10}A/m^2 . With this current density, a fiber with a $1 \mu\text{m}$ tip and thus $A_c = 0.78 \cdot 10^{-12} \text{m}^2$ cross-sectional area would be able to carry 7.8mA. Assuming that all fibers carry current, and to the same extend, 1 000, 10 000, and 100 000 fibers would be able to carry 7.8A, 78A, and 780A respectively.

This approach does not consider yet what is directly related to the intrinsic advantage of the fibers, which is to compensate for surface roughnesses and/or microscopic non-ideal centering/alignment. The non-uniform contact between the microfibers and the surface throughout the brush contact area will result in different contact resistances and thus non-uniform distribution of the currents through the fibers. Note that, in contrast to the situation with conventional carbon brushes, hot-spotting does not occur with the microfiber rings if designed properly. With

the fiber-resistance being a function of the fiber current, this is a recursive effect. To assess the orders of magnitudes, we assumed that only (1...10)% of the multitude of fibers assembled in parallel carry current *at the same time*. Then, 100 000, and 1 000 000 fibers are required to carry (0.78...7.8)A and (7.8...78)A respectively (Table III).

TABLE III
MICROFIBER CURRENT CARRYING CAPABILITIES FOR $1\mu\text{M}$ TIPS AND $10^{10}\text{A}/\text{M}^2$ CURRENT DENSITY

# fibers	conducting [%]	i_f [A]
100 000	1...10	0.78...7.8
1 000 000	1...10	7.8...78

B. Breakdown voltages

This topic is mostly relevant in the context of application of the microfiber rings for mitigation of discharge bearing currents. Therefore, we draw from results presented in [2]: Since the values for v_{bea} (Table II, Section V-B) are far below the Paschen minimum (Section III), v_{bea} could only be discharged by ESD through a path parallel to the bearing by exploiting the electric field emission effect. The electrically conducting tips of the conductive microfibers with very small diameters allow very small gap spacing and a geometry that results in local field enhancement are suitable to locally achieve the electric field strength for a breakdown to occur: (Here, “very small” refers to the dimensions that drives-engineers usually deal with.)

We approximate the results summarized above (Section III-C) with $V_b/d \approx 100\text{V}/\mu\text{m}$ and exploit the influence of local electrical field concentration with very sharp edges and thus with smaller tips to lower the V_b/d ratio: Without electric field distortion by dielectric materials around the electrode tips, approximating the field enhancement factor $\beta \propto r^{-1}$, where r is the radius of the tip, $V_b/d \approx 1\text{V}/\mu\text{m}$ can be found at $0.02\mu\text{m}$ tip diameter. Then, breakdowns at $\approx 2\text{V}$ would require gap spacings of $2\mu\text{m}$. With typical roughnesses of approximately 1.6 to $6.3\mu\text{m}$, this is at the low end of the surface roughnesses of machine shafts. Here, the mechanically flexible structure of the fibers plays in favorably, as the fibers can compensate these variations and reestablish electric contact the moment “good” electric contact is lost.

C. Voltage-current relationships

The current through the microfibers, i_f , is mainly a function of the voltage across the fibers, v_f , and the resistance between the microfibers and the shaft, R_f , which is itself a strong function of the current i_f . Furthermore, the resistance per individual fiber, $R_{f,1}$, will not be constant when the fiber is engaged with a moving surface. Aiming to assess the orders of magnitudes, we use the simplified assumption of R_f constant as a starting point and then investigate how the findings change with non-constant R_f .

1) *Assumption R_f constant:* From the measurements reported below (Section VIII-C) we take $R_{f,1} = 10\text{k}\Omega$. Then, $R_f = 0.1\Omega$ for 100 000 fibers, corresponding to $v_f = 0.1\text{V}$ at $i_f = 1\text{A}$; and $R_f = 0.01\Omega$ for 1 000 000 fibers, corresponding to $v_f(i_f = 1\text{A}) = 0.01\text{V}$ and $v_f(i_f = 10\text{A}) = 0.1\text{V}$. Assuming that only

(1...10)% of the multitude of fibers assembled in parallel do carry current *at the same time*, it is $R_f = (10...1)\Omega$ and $R_f = (1...0.1)\Omega$ for 100 000 and 1 000 000 fibers respectively. The corresponding voltage drops are $v_f(i_f = 1\text{A}, 100\,000\text{ fibers}) = (10...1)\text{V}$ and $v_f(i_f = 1\text{A}, 1\,000\,000\text{ fibers}) = (1...0.1)\text{V}$, as well as $v_f(i_f = 10\text{A}, 100\,000\text{ fibers}) = (100...10)\text{V}$ and $v_f(i_f = 10\text{A}, 1\,000\,000\text{ fibers}) = (10...1)\text{V}$ respectively (Table IV).

TABLE IV
MAGNITUDES OF MICROFIBER RING CURRENTS AND VOLTAGES FOR $R_{f,1} = 10\text{k}\Omega$ PER MICROFIBER

# fibers	conducting [%]	R_f [Ω]	i_f [A]	v_f [V]
100 000	100	0.1	1...10	0.1...1
1 000 000	100	0.01	1...10	0.01...0.1
100 000	1...10	10...1	1	10...1
100 000	1...10	10...1	10	100...10
1 000 000	1...10	1...0.1	1	1...0.1
1 000 000	1...10	1...0.1	10	10...1

The ranges of the voltage associated with these current-conduction scenarios are low, justifying the assumption of the constant current source and thus neglecting recursive effects for the analysis presented in Section VII-A.

2) *R_f not constant:* As larger currents are likely to contribute to building up of more current-conducting bridges and eventually leading to a “collapse,” R_f will decrease with increasing current. Simplified expressions of such characteristics could be $R_f = K_1/\sqrt{i_f}$, $R_f = K_2/i_f$, and $R_f = K_3/i_f^2$. If the values of the resistances for small currents are identical to the above case where R_f constant, the voltages v_f will even be smaller with R_f not constant than those identified above for R_f constant.

VII. THE PROPOSED CONCEPT IN THEORY - PART 2

A. Purpose “current-conduction”

For the analysis of the application of the microfiber rings for this purpose, we assume a constant current source and neglect recursive effects on the microfibers of the current generation. Then, the current-carrying capability becomes the main parameter of interest. Only in a second step, when recursive effects on the current generation are considered, the relationships $i_f = v_f(i_f)$ become important.

A comparison between Tables I and III shows that most of the currents can be readily carried with microfiber rings with 500 000 to 1 000 000, utmost 2 500 000, fibers, where the latter are more easily achieved with use of several microfiber rings in parallel. Furthermore, per the approach discussed above (Section VI-C) the ranges of the voltages associated with these currents and current-conduction scenarios are again so low that the assumption of the constant current source is justified.

B. Purpose “prevention of voltage build-up”

In order to protect the voltage sensitive impedance in parallel, v_f must not exceed a given threshold voltage. If used as mitigation technique for discharge bearing currents, the voltage across the bearing needs to be kept below a few Volts. In order to

determine the maximum current through the fibers, we set the resistance R_f to zero [2]. Then, the common-mode voltage is in parallel to the capacitance between the stator-winding and the rotor, C_{wr} , as the rotor is shorted to the frame of the machine (Fig. 6, where C_{wr} : rotor-to-winding capacitance, C_{rf} : rotor-to-frame capacitance, $C_{b,DE}$, $C_{b,NDE}$: drive-end and nondrive-end bearing capacitance). Taking by intention (very) high values for both the dv/dt of the common-mode voltage, $2kV/\mu s$, and the value of C_{wr} , $500nF$, we obtain a current of $2kV/\mu s \cdot 500nF = 1A$. This current is almost one order of magnitude smaller than the estimated current carrying capability with as few as 10 000 fibers when only 1% of the fibers are carrying current at the same time. Furthermore, for R_f from above, v_f can be readily kept below several Volts.

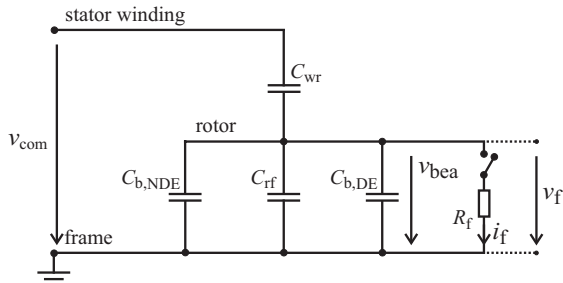


Fig. 6. Equivalent circuit for calculation of voltage and current of the microfiber ring when used for prevention of voltage build-up across the bearing.

VIII. EXPERIMENTAL RESULTS

A. Test set-up for purpose “current conduction”

A test-setup was constructed using an off-the shelf four-pole 60Hz 230V/460V 10HP squirrel cage induction motor mounted on an electrically insulated test bench and supplied by an off-the shelf 3phase 460V PWM controlled voltage-source inverter (Fig. 7). The motor was only grounded through its shaft so that all generated high-frequency common-mode current I_{com} (2) was forced to return to ground through the shaft grounding connection(s). These grounding connections could be given (i) either through a bearing (deep groove ball bearing type 6207), (ii) a bearing and a microfiber ring (312 000 fibers) assembled in parallel, or (iii) a microfiber ring only.

The results are shown in Fig. 8: The current carrying capability of the microfiber grounding ring is essentially constant as the motor speed increases, while the one of the bearing decreases with increasing motor speed. The conductive microfiber grounding rings provide a reliable conduction contact independently of the motor speed. When the microfiber ring and the bearing are simultaneously grounded, the microfiber ring carries approximately the same amount of current at 120rpm and approximately three times more than the bearing at 600rpm motor shaft speed. At 1800rpm and 3600rpm, almost all current is carried by the microfiber ring, and the current through the bearing is negligible. These test results confirm that the microfiber grounding ring is effectively able to carry currents with frequencies and magnitudes typical for high-frequency circulating bearing and common-mode currents (if necessary, use of more fibers per ring and/or several rings in parallel).

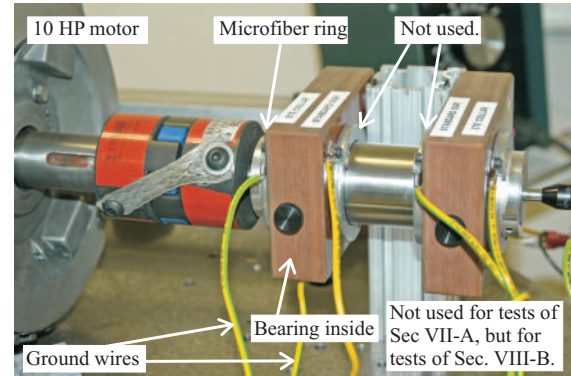


Fig. 7. Test set-up for the measurement of the microfiber ring current-conduction capability at typical ground-current waveforms.

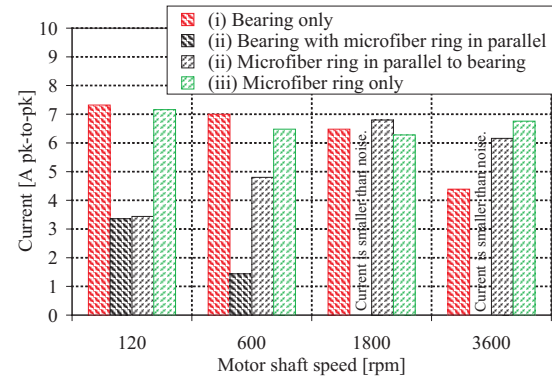


Fig. 8. Measured currents through the bearing and/or the microfiber ring with (i) only the bearing connected, (ii) both the bearing and the microfiber ring connected in parallel, (iii) only the microfiber ring connected (test set-up shown in Fig. 7).

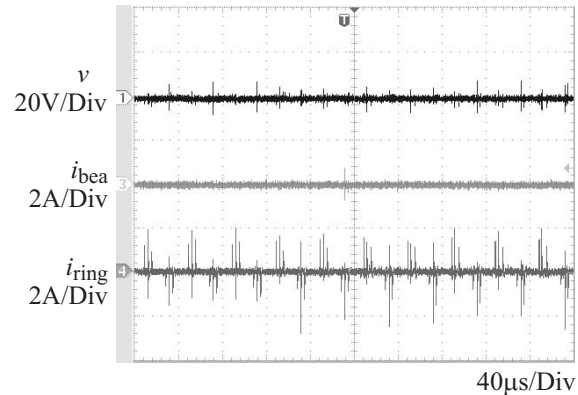


Fig. 9. Measured voltage and currents with bearing and microfiber ring assembled in parallel and at 600rpm (test set-up shown in Fig. 7).

B. Test set-up for purpose “prevention of voltage build-up”

The ability of rings of conductive microfibers to prevent a voltage of several Volts to build up across the bearing was verified with a series of tests. The tests were carried out with two four-pole 50/60Hz 230V/460V off-the-shelf squirrel-cage induction motors with 1HP and 10HP rated power, and two off-the-shelf 460V voltage-source inverters, considering different motor speed, variable switching frequency, and additional grease (“contamination”) on the motor shaft. These tests have been

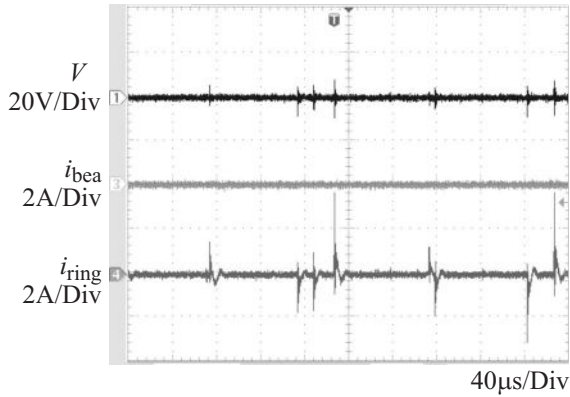


Fig. 10. Measured voltage and currents with bearing and microfiber ring assembled in parallel and at 1800rpm (test set-up shown in Fig. 7).

reported on in [2], confirming that the microfiber rings can prevent the voltage across the bearing to build up to levels where the bearing is endangered, as the bearing is shorted through a parallel low-resistance path. Exemplarily, Fig. 11 shows the measured waveforms of v_{com} and v_{bea} of the same test setup as Fig. 5, but now a ring of conductive microfibers is applied. When comparing the two figures, it can be seen that the voltage across the bearing is reduced to a maximum of 2V.

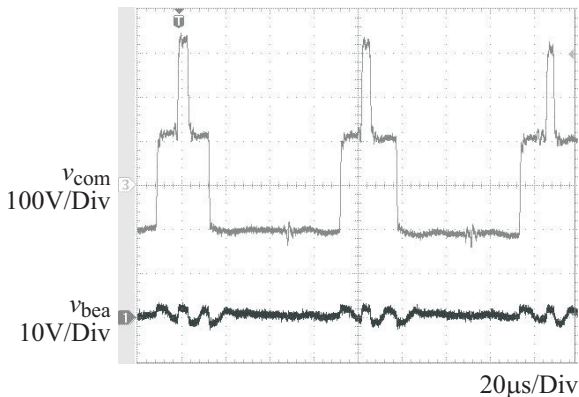


Fig. 11. Common-mode voltage, v_{com} , and voltage across the bearing, v_{bea} with ring of conductive microfibers; squirrel-cage induction motor, 215TC frame, 10HP rated power, motor speed 1800r/min, compare with Fig. 5.

C. Test set-up for purpose “voltage-current relationship”

The right side of the test set-up shown in Fig. 7, along with a 60Hz 1.4kVA 10A power-supply was used to measure the voltage-current relationship of the microfiber rings at 60Hz and with currents from 2 to 14Arms. To this aim, the rotating shaft was electrically isolated from the motor shaft, two microfiber rings were connected in series, and voltage was applied to the rings. The test results show again the capability of the microfibers to carry high currents as they can occur as parasitic currents in variable frequency drive motors. The measured voltages (Fig. 12) are in line with the order of magnitude identified above (Section VI-C), and the influence of the motor shaft speed on the microfiber performance is only small. The resistances per

microfiber ring for the different current amplitudes and shaft speed are derived from these measurements (Fig. 13). The values decrease with increasing current, what is again in line with the above statements (Section VI-C). The figure illustrates well how the microfiber performance increases with increasing current magnitude. The exact voltage-current relationship, including the influence of the current frequency and the motor shaft surface speed requires more research to understand the nature.

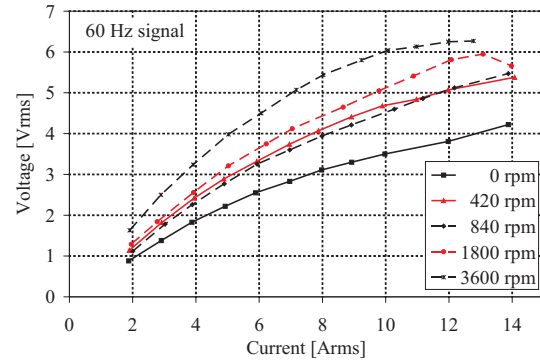


Fig. 12. Measured voltage-current relationship for two microfiber rings in series and at 60Hz signals.

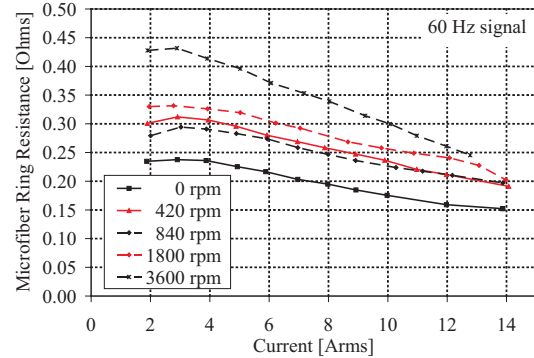


Fig. 13. Resistance per microfiber ring at 60Hz signals computed from the results shown in Fig. 12.

IX. CONCLUSION

A new brush concept made from millions of conductive microfibers has been presented. With this technique, a high density of contact points given by a multitude of conductive microfibers that are arranged in parallel via a supporting ring can be used to provide many parallel paths for both (A) conduction of current of several 10s of Amperes and (B) discharge of voltages of only a few Volts. If properly designed, such brushes can meet all the demands on carbon brushes but exclude the problems of excessive wear and hot-spotting/thermal wear commonly quoted with the first. These brushes have negligible frictional wear, are free of maintenance, and robust towards contamination. In addition, they are especially suitable for use with high-frequency currents and voltages, as they also allow current-conduction based on electric field emission. Design criteria for such brushes were developed and the orders of magnitudes involved identified. The theoretical results were supported by measurements.

APPENDIX

Appendix A: List of abbreviations

Acronym	Definition
BVR	Bearing Voltage Ratio
CM	Common-mode
EDM	Electric Discharge Machining
ESD	Electrostatic Discharge
F-N	Fowler-Nordheim
HF	High-frequency
HP	Horse Power

Appendix B: List of symbols

Name	Description
d	gap spacing
p	pressure
i_f	current through microfiber ring
i_{com}	high-frequency common-mode current
v_{bea}	voltage across the bearing
v_{com}	common-mode voltage
v_f	voltage across microfiber ring
v_{Lg}	line-to-ground voltage
A_c	cross-sectional area
$C_{b,DE}$	drive-end bearing capacitance
$C_{b,NDE}$	nondrive-end bearing capacitance
C_{rf}	rotor-to-frame capacitance
C_{wr}	rotor-to-winding capacitance
I	current
I_{com}	maximum amplitude the HF common-mode current
E	electric field-strength
E_m	microscopic electric field-strength at the microscopic surface of the contact
R_f	resistance between the microfibers and the shaft
$R_{f,1}$	per-fiber resistance between an individual microfiber and the shaft
V	voltage
V_B	breakdown voltage
β	total electric field enhancement factor
β_g	geometric electric field enhancement factor
β_m	microscopic electric field enhancement factor
ρ	pressure-gap product

REFERENCES

[1] M.D. Bryant, "Tribology issues in electric contacts," lecture notes ME 383S, Lubrication, Wear & Bearing Technology, University of Texas at Austin, 2006.

[2] A. Muetze and H.W. Oh, "Application of static charge dissipation to mitigate electric discharge bearing currents," *Proceedings 5th IEEE 5th International Electric Machines and Drives Conference (IEMDC 2007)*, pp. 1059-1066, Antalya, Turkey, May 2-5, 2007.

[3] F. Paschen, "On sparking over in air, hydrogen, carbon dioxide under the potentials corresponding to various pressures," *Wiedemann Annalen der Physik und Chemie*, vol. 37, pp. 69-96, 1889.

[4] J.M. Meek and J.D. Craggs, *Electrical breakdown of gases*, John Wiley and Sons, New York, 1978.

[5] H. Raether, *Electron avalanches and breakdown in gases*, Butterworth, London, 1964.

[6] I. Gallimberti, "The mechanism of the long spark formation," *Journal de Physique*, vol. 40, no. C7, pp.193-250, July 1979.

[7] E.M. Bazelyan and Y.P. Raizer, *Spark discharge*, CRC Press, Florida, 1997.

[8] A. Wallash, "Electric breakdown and ESD phenomena for devices with nanometer-to-micron gaps," *Proceedings of The International Society for Optical Engineering, Conference on Reliability, Testing, and Characterization for MEMS/MOEMS II*, vol. 4980, no. 16, pp. 87-98, January 2003.

[9] R.M. Schaffert, *Electrophotography*, John Wiley and Sons, 1975.

[10] A. Wallash and T. Hughbanks, "Capacitive coupling effects in spark gap devices," *Proceedings of 16th Electrical Overstress and Discharge (EOS/ESD) Symposium*, EOS/ESD Association, pp. 273-278, 1994.

[11] R.H. Fowler and L. Nordheim, "Electron emission in intense electric fields," *Proceedings Royal Society London, Series A, Containing Papers of Mathematical and Physical Character*, vol. 119, no. 781, pp. 173-181, May 1928.

[12] T.E. Stern, B.S. Gossling, and R.H. Fowler, "Further studies in the emission of electrons from cold metals," *Proceedings Royal Society London, Series A, Containing Papers of Mathematical and Physical Character*, vol. 124, no. 795, pp. 699-723, July 1929.

[13] F. Gomer, *Field emission and field ionization*, Harvard University Press, 1961.

[14] C.A. Spindt, I. Brodie, L. Humphrey, and E.R. Westerberg, "Physical properties of thin-film field emission cathodes with molybdenum cones," *Journal of Applied Physics*, vol. 47, no. 12, pp. 5248-5263, December 1976.

[15] P.G. Slade and E.D. Taylor, "Electrical breakdown in atmospheric air between closely spaced (0.2 μm -40 μm) electrical contacts," *IEEE Transactions on Components and Packaging Technologies*, vol. 25, no. 3, pp. 390-396, September 2002.

[16] R.T. Lee, H.H. Chung, and Y.C. Chiou, "Arc erosion of silver electric contacts in a single arc discharge across a static gap," *IEEE Proceedings Science, Measurement and Technology*, vol. 148, no. 1, pp. 8-14, January 2001.

[17] J.M. Torres and R.S. Dhariwal, "Electrical field breakdown at micrometre separations," *Nanotechnology*, vol. 10, no. 1, pp. 102-107, March 1999.

[18] S. Chen, T.A. Lipo, and D. Fitzgerald, "Modelling of motor bearing currents in inverter drives," *IEEE Transactions on Industry Applications*, vol. 32, no. 6, pp. 1365-1370, November/December 1996.

[19] D. Busse, J. Erdman, R. Kerkman, and D. Schlegel, "Bearing currents and their relationship to PWM drives," *IEEE Transactions on Power Electronics*, vol. 12, no. 2, pp. 243-252, March 1997.

[20] D. Busse, J. Erdman, R. Kerkman, D. Schlegel, and G. Skibinski, "System electrical parameters and their influence effect on bearing currents," *IEEE Transactions on Industry Applications*, vol. 33, no. 2, pp. 577-584, March/April 1997.

[21] D. Busse, J. Erdman, R. Kerkman, D. Schlegel, and G. Skibinski, "Characteristics of shaft voltage and bearing currents," *IEEE Industry Applications Magazine*, vol. 3, no. 6, pp. 21-32, November/December 1997.

[22] P. Link, "Minimizing electric bearing currents in ASD systems," *IEEE Industry Applications Magazine*, vol. 5, no. 4, pp. 55-66, July/August 1999.

[23] H.E. Boyanton and G. Hodges, "Bearing fluting," *IEEE Industry Applications Magazine*, vol. 8, no. 5, pp. 53-57, September/October 2002.

[24] R. Naik, T.A. Nondahl, M.J. Melfi, R.F. Schiferl, and J.S. Wang, "Circuit model for shaft voltage prediction in induction motors fed by PWM-based AC drives," *IEEE Transactions on Industry Applications*, vol. 39, no. 5, pp. 1294-1299, September/October 2003.

[25] R.F. Schiferl, M.J. Melfi, "Bearing current remediation options," *IEEE Industry Applications Magazine*, vol. 10, no. 4, pp. 40-50, July/August 2004.

[26] A. Muetze and A. Binder, "Don't lose your bearings - mitigation techniques for bearing currents in inverter-supplied drive systems," *IEEE Industry Applications Magazine*, vol. 12, no. 4, pp. 22-31, July/August 2006.

[27] A. Muetze and A. Binder, "Calculation of motor capacitances for prediction of discharge bearing currents in machines of inverter-based drive systems," *Proc. of 5th IEEE International Electric Machines and Drives Conference (IEMDC)*, pp. 264-270, San Antonio, TX, May 15-18, 2005; to appear in *Transactions on Industry Applications*.

[28] A. Muetze and A. Binder, "Calculation of circulating bearing currents in machines of inverter-based drive systems," *IEEE Transactions on Industrial Electronics*, vol. 54, no. 2, pp. 932-938, April 2007.

[29] *Guide to the Selection of The Surface Finish of Stainless Steel on Fabricated Items*, Solids Handling and Processing Association (SHAPA) Technical Bulletin No. 1, January 2000.